JOURNAL OF Materials CHEMISTRY

New (Ni, Co)-based layered double hydroxides with intercalated oxometalate (Mo, W) species, obtained by *chimie douce* reactions†

Christophe Vaysse, Liliane Guerlou-Demourgues, Alain Demourgues, Florian Lazartigues, David Fertier and Claude Delmas*

Institut de Chimie de la Matière Condensée de Bordeaux-CNRS and Ecole Nationale Supérieure de Chimie et Physique de Bordeaux, 87 Av. Dr A. Schweitzer, 33608 Pessac cedex, France. Tel: +33-5-5684-6296; Fax: +33-5-5684-6634; E-mail: delmas@icmcb.u-bordeaux.fr

Received 29th August 2001, Accepted 16th January 2002
First published as an Advance Article on the web 13th February 2002

Layered double hydroxides (LDHs), containing intercalated oxometalate (Mo, W) species, were obtained by *chimie douce* reactions from $NaNi_{1-y}Co_yO_2$ cobalt substituted sodium nickelates ($0.10 \leqslant y \leqslant 0.40$). The X-ray diffraction (XRD), infrared (IR) and extended X-ray absorption fine structure (EXAFS) studies show that, in both cases, $M_2O_7^{2-}$ anions (M=Mo, W), made of corner-sharing tetrahedra, are intercalated. In these MO_4 tetrahedra, the M–O bond with the bridging oxygen is elongated compared to the other ones, and the M–O–M angle is close to 115°. Oxygen atoms belonging to water molecules are pointing to some faces of the MO_4 tetrahedra. The presence of such peculiar intercalated species, as well as the existence of an hydrogen bond network, leads to local distortions within the slabs, which entails a "turbotratic type" shape of the XRD patterns.

Introduction

Much attention has been devoted in recent years to layered double hydroxides (LDHs), which exhibit interesting anionic exchange properties and can be used as electrode materials or precursors of new catalytic materials.[1,2] The structure of these materials consists of stacked brucite-type $[M^{II}_{1-y}L^{III}_y(OH)_2]$ slabs. The excess positive charge, due to partial substitution of trivalent cations (L) for the divalent cations (M), is compensated by X^{n-} anions, intercalated within the interslab space, together with water molecules. This leads to the following general formula:[1,3]

$$[M^{II}_{1-y}L^{III}_y(OH)_2]^{y+}X^{n-}_{y/n}[H_2O]_z.$$

The structure is stabilised by the electrostatic interactions between the slabs and the X^{n-} anions, as well as by a strong hydrogen bond network between the water molecules, the anions and the slab hydroxyls.

The most common method for preparing LDHs is the coprecipitation method. It is based on the slow addition of an alkaline solution to a solution of divalent and trivalent metal salts, mixed in the suitable ratio. The pH is maintained at a selected value in order to achieve simultaneous precipitation of both divalent and trivalent metals into a monophasic mixed hydroxide. The main drawback of this method consists of the possible discrepancy between the divalent to trivalent metal ratio within the final precipitated material, and the solution composition before the precipitation. Which is why controlling the amount of inserted anions in such conditions is very difficult.

In order to solve these problems, an original preparation method, involving several *chimie douce* topotactic reaction steps, was developed in our laboratory a few years ago. This method consists of a first step of decoupling the building of the $M_{1-y}L_yO_2$ slabs, which is performed by solid state chemistry at high temperature, and a second step of anionic intercalation, which is coupled with redox reactions. LDHs, with the typical formula: $[Ni^{II}_{1-y}Co^{III}_y(OH)_2]^{y+}X^{n-}_{y/n}[H_2O]_z$ (X^{n-} = CO_3^{2-}, SO_4^{2-}, NO_3^-, OH^-, $(VO_3)^{n-}$), were obtained.[4,5] The intercalation of acrylate anions was very recently performed in such materials by this method; it was followed by *in situ* polymerisation of the monomer entities.[6] The amount of inserted anions is directly related to their own negative charge (n) and to the L trivalent cation concentration within the slabs. This method is derived from the one already used in the laboratory to obtain cobalt or iron substituted nickel hydroxides, which were intended to be used as positive electrode materials in nickel–cadmium, nickel–hydrogen or nickel–metal hydride batteries.[7–9] Nevertheless, this method also suffers from several limitations: (i) the presence of 3d cations with various oxidation states, and (ii) the existence of the high temperature stable starting layered oxide.

The main goal of the present work consisted of inserting large anionic species, which may create large cavities, suitable for catalytic reactions within the interslab space. Molybdate and tungstate species, which exhibit a potential interest for catalytic applications, appeared as good candidates for intercalation in LDHs, as reported by Sels *et al.*,[10,11] Gardner and Pinnavaia,[12] and Tatsumi *et al.*,[13] for WO_4^{2-}, $W_7O_{24}^{6-}$ and $W_{12}O_{40}^{10-}$ species, respectively, and by several authors for $Mo_7O_{24}^{6-}$ anions.[14–16] LDHs, with such intercalated species, were prepared by these authors using ion exchange reactions from terephthalate-pillared magnesium–aluminium or zinc–aluminium LDHs. The exchange of the initially inserted terephthalate anion was achieved in tungstate or molybdate aqueous solution at pH 4–5.

The present work concerns the intercalation of molybdate and tungstate anions into LDHs, based on $Ni_{1-y}Co_y(OH)_2$ slabs (y = 0.10–0.40). Special attention is devoted to the materials that are obtained for y = 0.30.

†Electronic supplementary information (ESI) available: parameters obtained after refinement of the EXAFS data at the Ni and Mo K-edges for $LDH_{0.30}$(Mo) (Table S1) and parameters obtained after refinement of the EXAFS data at the W L(III)-edge for $LDH_{0.30}$(W) (Table S2). See http://www.rsc.org/suppdata/jm/b1/b107791k/

DOI: 10.1039/b107791k

Experimental

The preparation procedure has previously been described in detail elsewhere.[8,17] It consists of three steps: classical solid state reaction at high temperature, oxidising hydrolysis and reduction.

The $NaNi_{1-y}Co_yO_2$ cobalt substituted sodium nickelate ($y = 0.10$–0.40) is prepared at 750 °C and is used as the starting material for the *chimie douce* reactions. The γ-oxyhydroxide is then prepared by an oxidising hydrolysis of the $NaNi_{1-y}Co_yO_2$ phase, in an oxidising aqueous solution (5 M KOH, 0.8 M NaClO). The third step, the reduction, is described in detail hereafter. Several procedures, which lead to the insertion of molybdate and tungstate anions, are presented.

Preparation of the LDHs by reduction of the γ-oxyhydroxide in the presence of Na_2WO_4

The reduction of the γ-oxyhydroxide is performed with H_2O_2, which allows the selective reduction of nickel to the divalent state and of cobalt to the trivalent state.[18] The role of Na_2WO_4 is to supply, into the reaction medium, tungstate species, which are the candidates to be intercalated, in order to compensate for the excess positive charge in the slab.

1 g of γ-oxyhydroxide is dispersed in a solution containing 4 g of $Na_2WO_4{\cdot}2H_2O$ in 500 mL of distilled water. The reduction is carried out by adding 50 mL of 5 M H_2O_2 to this solution. Due to the basic pH conditions (pH ≈ 10), very unstable $[W(O_2)_4]^{2-}$ peroxotungstate species are formed in the reaction medium.[19] In order to form stable anionic tungsten species, the pH has to be decreased. Acetic acid, CH_3COOH, was chosen as the acid agent (pH ≈ 5), because its parasitic insertion into the final LDH turned out to be negligible. Indeed, additional experiments have shown that HCl, as an example, leads to a non-desirable intercalation of Cl^- ions. After 24 h stirring, the obtained material is filtered, washed with distilled water and dried at 40 °C. The LDH phases, obtained in the presence of Na_2WO_4, are denoted as $LDH_y(W)$, y being the cobalt amount in the slab.

From a general point of view, when the reduction step is performed in air, carbonate ions are present in the reaction medium and tend to be preferentially intercalated into the interslab space at the expense of other species in the solution, like SO_4^{2-}, NO_3^-, Cl^-, ClO_4^-, CH_3COO^- anions.[4,20] In the present work, the reduction step was carried out in air and despite this no parasitic insertion of carbonate anions was observed. This behaviour, very surprising at first sight, will be commented on in the next section.

Preparation of the LDHs by reduction of the γ-oxyhydroxide in the presence of $(NH_4)_6Mo_7O_{24}$

In this case, the reduction must be performed in an air-free atmosphere (in a glove box under an argon atmosphere), in order to prevent any parasitic intercalation of carbonate anions. 3 g of $(NH_4)_6Mo_7O_{24}{\cdot}2H_2O$ are dissolved in 100 mL of doubly distilled water, and 1 g of γ-oxyhydroxide is then dispersed in the suspension. 20 mL of 5 M H_2O_2 are then added dropwise into the solution. Contrary to the tungstate materials, no acidification of the reduction medium is necessary in this case, because the peroxomolybdate species are stable in the solution. After 24 h stirring, the obtained material is filtered, washed and dried at 40 °C under an argon atmosphere. The obtained materials are denoted as $LDH_y(Mo)$.

Preparation of the tungstate and molybdate intercalated LDHs by exchange reactions from $LDH_{0.30}(CO_3)$

Carbonate material. 4 g of Na_2CO_3 are dissolved in 100 mL of distilled water, and 1 g of γ-oxyhydroxide is then dispersed in the solution. 20 mL of 5 M H_2O_2 are then added dropwise into the solution. The material is stirred for 24 h, filtered, washed with distilled water and dried in an air atmosphere. This material is used as the precursor for the exchange reactions.

Tungstate material. 1 g of $LDH_{0.30}(CO_3)$ is added to 250 mL of distilled water. 4 g of Na_2WO_4 are dissolved in the solution, and the pH is brought down to 5 by adding CH_3COOH. 50 mL of 5 M H_2O_2 are then added, in order to have the same peroxotungstate species in the solution as for the material prepared by direct reduction of the γ-oxyhydroxide phase. The material is stirred for 24 h, filtered, washed with distilled water and dried in air.

Molybdate material. 1 g of $LDH_{0.30}(CO_3)$ is added to 100 mL of doubly distilled water. 3 g of $(NH_4)_6Mo_7O_{24}$ are dissolved in the solution, and 20 mL of 5 M H_2O_2 are added. The material is stirred for 48 h, filtered, washed with doubly distilled water and dried in an argon atmosphere.

Characterisation techniques

The X-ray diffraction (XRD) patterns were recorded on an INEL X-ray diffractometer, equipped with a cobalt anticathode, a forward monochromator and a CPS 120 curved sensitive detector.

The Fourier transform infrared (FTIR) spectra were obtained by using a PerkinElmer Spectrum One spectrophotometer, equipped with a diffuse reflectance sphere. The materials were dispersed and gently ground in KBr powder, placed in the diffuse reflectance sphere and analysed.

Chemical analyses were performed by inductively coupled plasma (ICP) emission spectroscopy for Ni, Co, W and Mo and by elementary organic microanalysis for C and H, at the CNRS facility in Vernaison.

The X-ray absorption measurements were carried out on beam line XAS4 at the Laboratoire pour l'Utilisation du Rayonnement Electromagnétique (LURE) in Orsay (France). Ni and Mo K absorption edges and W L(III)-edge (8333 eV, 20000 eV and 10207 eV, respectively) were investigated. A Si(111) monochromator was used for energy selection, leading to a resolution of 2 eV. In any case, a scan of the energy was performed from 100 eV below to 1000 eV above the edges ($\Delta k \approx 16$ Å^{-1}). All the experiments were undertaken at room temperature.

Results and discussion

The present paper deals with the characterisation of the $LDH_y(Mo)$ and the $LDH_y(W)$ phases by XRD, IR spectroscopy, chemical analysis and extended X-ray absorption fine structure (EXAFS) spectroscopy, aiming at determining the structure of the interslab species.

XRD study of the materials obtained by direct reduction

The various materials involved in the *chimie douce* reactions were characterised successively.

Sodium nickelate and γ-oxyhydroxide. Depending on the amount of Co, the $NaNi_{1-y}Co_yO_2$ precursor phases crystallise either in the trigonal system (space group (SG): $R-3m$), for $y = 0.20$–0.40, or in the monoclinic system, for $y = 0.10$. The slab oxygen layers exhibit an O3 type packing (AB CA BC) in the former case, which becomes O′3 (distorted O3) in the latter case.[21] The interslab distance is close to 5.2 Å for all materials.

Starting from the nickelate phases, oxidation of the metal ions of the slabs, partial exchange of Na^+ ions for protons and K^+ ions, as well as intercalation of water molecules occur during the oxidising hydrolysis step, leading to the

γ-oxyhydroxide phases.[8,22] These materials crystallise in the trigonal system (SG: *R*3*m*), with a P3 oxygen packing type (AB BC CA), which implies a slab gliding, as compared to the O3 packing of the nickelate precursor phases. As a result of the oxidation of the metal ions, the metal–metal intraslab distance is lower in the γ-phases than in the nickelate phases and, in addition, the interslab distance is strongly increased up to 7 Å, due to the intercalation of water molecules and potassium ions.

The LDH. The XRD patterns of the $LDH_y(Mo)$ (y = 0.10–0.40) and the $LDH_{0.30}(W)$ phases are displayed in Fig. 1. The results, obtained for the other $LDH_y(W)$ compositions (y = 0.10, 0.20 and 0.40), lead to similar results to those observed for molybdate-intercalated materials, and are not presented here. The diagram of $LDH_{0.30}(CO_3)$ is also given in Fig. 1 for comparison purposes. The $LDH_{0.30}(CO_3)$ phase crystallises in the trigonal system (SG: *R*3*m*) with a P3 oxygen packing, like in the case of the γ-oxyhydroxide phase. Indexation of its X-ray diagram can be performed with a hexagonal cell, with three slabs per cell, as reported in Fig. 1. The interreticular distance of the (003) line corresponds to the interslab distance, while the interreticular distance of the (110) line represents half the metal–metal distance. From a general point of view, the lines of the XRD patterns of $LDH_y(Mo)$ seem sharper than those of the $LDH_{0.30}(W)$ phase, suggesting a better crystallisation state. The (10*l*) and (11*l*) line series, observed for $LDH_{0.30}(CO_3)$, are replaced, for $LDH_y(Mo)$ and $LDH_{0.30}(W)$, by two large and asymmetric bands in the 30–45° and 60–65° ($2\theta_{Cu}$) ranges. This is characteristic of some disorder in the periodicity of the slabs. Such a phenomenon can be related either to local distortions within the slabs, as already demonstrated in $LDH(VO_3)$[5] and LDH(acrylate),[23] or to a turbostratic effect, *i.e.* a misorientation of the slabs which are packed along the c axis. This is induced by the large interslab distance, which weakens the bonding interactions between the interlayer species and the host lattice. As a consequence of the turbostratic-like character, no indexation of the XRD patterns is possible. Nevertheless, by analogy with the diagram of $LDH_{0.30}(CO_3)$, the first two peaks can be considered as characteristic of the interslab distance, while the peak around 60° is characteristic of the metal–metal intraslab distance.

The absence of any peak at 7.7 Å, which would be the signature of a parasitic $LDH_y(CO_3)$ phase, must be noticed. This is surprising in the case of $LDH_{0.30}(W)$, because the preparation of the material is performed in an air atmosphere, which usually promotes the preferential intercalation of carbonate ions.[20] The results obtained for $LDH_{0.30}(W)$ may be attributed to the acidic pH of the reaction medium (pH = 5), which is unfavourable to the presence of carbonate ions, and, as the most important factor, to the fact that carbonate ions may be trapped in the aqueous solution. The peroxotungstate anions are indeed likely to be associated to carbonate anions in order to form $[W_4O_8(O_2)_6(CO_3)]^{6-}$ species, which were reported by Stomberg.[24] The carbonate anions are thus trapped in such species, which cannot be intercalated as a result of their too large size.

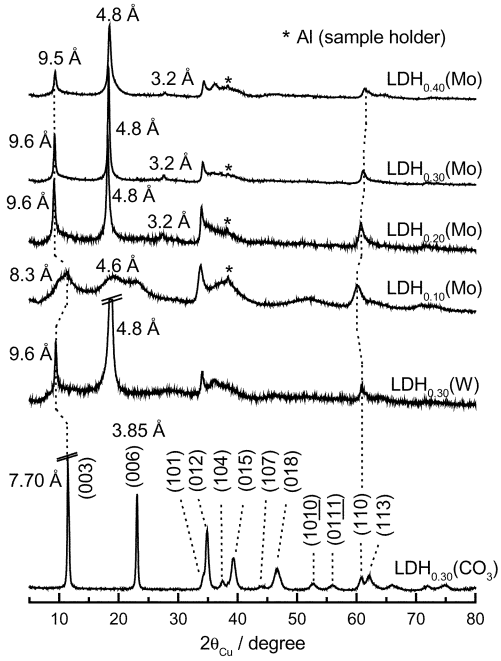

Fig. 1 XRD patterns of $LDH_y(Mo)$ (y = 0.10–0.40) and $LDH_{0.30}(W)$. $LDH_{0.30}(CO_3)$ is given for comparison.

On the diagrams of the $LDH_y(Mo)$ (y = 0.20–0.40) and $LDH_{0.30}(W)$ materials, as well as on that of $LDH_{0.30}(CO_3)$, the interplanar distances relative to the first two peaks are twice one another, which indicates that the Ni-based slabs are regularly spaced along the c axis, with fixed interslab distances (ranging from 9.0 to 9.6 Å). It should be noticed that the distances reported in the literature for $Mo_7O_{24}^{6-}$ (or $W_7O_{24}^{6-}$)-intercalated LDHs (12–12.5 Å) are significantly larger than those found in this study, suggesting that the nature and/or the arrangement of the inserted oxometalate entities are different.[12,14–16] In the case of $LDH_{0.10}(Mo)$, the interplanar dis- tances relative to the first two peaks are not twice one another, which is characteristic of an interstratification phenomenon. Such behaviour, already observed in the case of manganese-substituted hydroxides,[25,26] corresponds to a statistical stacking, along the *c* axis, of different motives, involving different occupancies of the interslab space. The low amount of the intercalated species should lead them to segregate in certain domains, which should exhibit a large interslab space close to 9.0–9.6 Å, while other interslab space domains should stay "empty", with an interslab distance close to 4.6 Å (as in β(II)-$Ni(OH)_2$).

Besides, as compared to the behaviour of $LDH_{0.30}(CO_3)$, the XRD patterns of the $LDH_y(Mo)$ and the $LDH_{0.30}(W)$ phases exhibit an inversion of the first two diffraction lines intensities. This behaviour will be commented on in the Discussion section and correlated to the structural features and the location of the intercalated species.

In order to identify the molybdate or tungstate intercalated species, chemical analyses on $LDH_{0.30}(Mo)$ and $LDH_{0.30}(W)$, which exhibit no structure interstratification, have been performed.

Chemical analysis

The A : (Ni + Co) atomic ratios (where A designates a given element), calculated on the basis of the weight percentage values, are reported in Table 1 for $LDH_{0.30}(Mo)$ and for $LDH_{0.30}(W)$. The values of the Mo : (Ni + Co) and W : (Ni + Co) molar ratios (0.30 and 0.26, respectively) confirm the effective insertion of molybdate and tungstate species into the LDHs, already suggested by XRD.

$LDH_{0.30}(Mo)$. It should be noted that, in this material family, the nickel ions are divalent, while the cobalt ions are trivalent.[22] On account of the Mo : (Ni + Co), Ni : (Ni + Co) and Co : (Ni + Co) ratios, the achievement of the electroneutrality within the material requires that 0.29 negative charge must be brought by the oxomolybdate anions, which corresponds to around one negative charge per molybdenum atom. This suggests the presence of $Mo_2O_7^{2-}$ entities, which were reported as an example in $MgMo_2O_7$.[27] This entity is constituted of two corner sharing MoO_4 tetrahedra, like $Cr_2O_7^{2-}$. The hypothesis of MoO_4^{2-}, $Mo_3O_{10}^{2-}$ or Mo_3O_9 entities must be rejected for charge consideration. The very weak carbon amount is in agreement with the results of XRD, which has not

Table 1 Values of the experimental and calculated A : (Ni + Co) molar ratios for various A elements in the $LDH_{0.30}(W)$ and the $LDH_{0.30}(Mo)$ phases

$LDH_{0.30}(Mo)$	A	Ni	Co	Mo	C	H
	Weight (%)	26.03	10.93	18.10	0.32	2.18
	A : (Ni + Co) molar ratio	0.71	0.29	0.30	0.04	3.47
	Calculated weight (%)[a]	27.04	11.09	18.68	0.31	2.27
$LDH_{0.30}(W)$	A	Ni	Co	W	C	H
	Weight (%)	23.90	9.02	26.75	0.66	2.00
	A : (Ni + Co) molar ratio	0.72	0.28	0.26	0.10	3.57
	Calculated weight (%)[b]	24.72	9.65	27.97	0.70	2.10

[a]The calculated values correspond to the hypothetical formula, deduced from experimental results $Ni_{0.71}Co_{0.29}(OH)_2(Mo_2O_7)_{0.15}(H_2O)_{0.59}(CO_3)_{0.04\ (adsorbed)}$. [b]The calculated values correspond to the hypothetical formula, deduced from experimental results $Ni_{0.72}Co_{0.28}(OH)_2(W_2O_7)_{0.13}(CH_3COO)_{0.02}(H_2O)_{0.71}(CH_3COO)_{0.03(adsorbed)}$.

shown the presence of an additional $LDH_{0.30}(CO_3)$ phase, which would be characterised by a diffraction line at 7.7 Å. The IR study, presented in the next section, reveals a weak $\nu_3(CO_3)$ vibration band, indicating the presence of few carbonate anions. The C element will therefore be considered in the following as present in adsorbed "carbonate species", which are not taken into consideration for the charge compensation, since they must be protonated or physisorbed as CO_2. The chemical formula can be written as follows: $Ni_{0.71}Co_{0.29}(OH)_2(Mo_2O_7)_{0.15}(H_2O)_{0.74}(CO_3)_{0.04(adsorbed)}$.

The percentages of the various elements, calculated on the basis of this formula, are in good agreement with the experimental ones, as shown in Table 1.

$LDH_{0.30}(W)$. On the basis of the molar values, gathered in Table 1, it turns out that the 0.28 negative charge, required for charge compensation, is brought by the tungstate ions, which corresponds to around one negative charge per tungsten atom, and leads to the proposal of a $W_2O_7^{2-}$ entity, similar to $Mo_2O_7^{2-}$. The value of the C : (Ni + Co) molar ratio (0.10) is significant. The absence of the $\nu(CO_3)$ vibration band on the $LDH_{0.30}(W)$ IR spectrum, presented in Fig. 2 and discussed in the next section, suggests that the C element cannot be attributed to co-intercalated or adsorbed carbonate ions. It may be due to acetate anions, coming from the reaction medium, where acetic acid was added in order to decrease the solution pH. A part of these anions (0.02) may be co-inserted with tungstate entities, in order to compensate the 0.02 missing negative charges, which are not brought by the tungstate entities. The other part (0.03) may be adsorbed on the grain surface, and will not be taken into consideration for the charge compensation, since they must be protonated or physisorbed as CH_3COOH. Note that this separation in two types of acetate ions was done just to establish the chemical formula although its real meaning is questionable. The general formula can therefore be written as: $Ni_{0.72}Co_{0.28}(OH)_2(W_2O_7)_{0.13}(CH_3COO)_{0.02}(H_2O)_{0.71}(CH_3COO)_{0.03(adsorbed)}$ The element percentages, calculated from this formula, are in agreement with the experimental ones again (Table 1).

In order to verify the presence of the $Mo_2O_7^{2-}$ and $W_2O_7^{2-}$ intercalated anions in the LDHs, an IR study has been performed for all the materials.

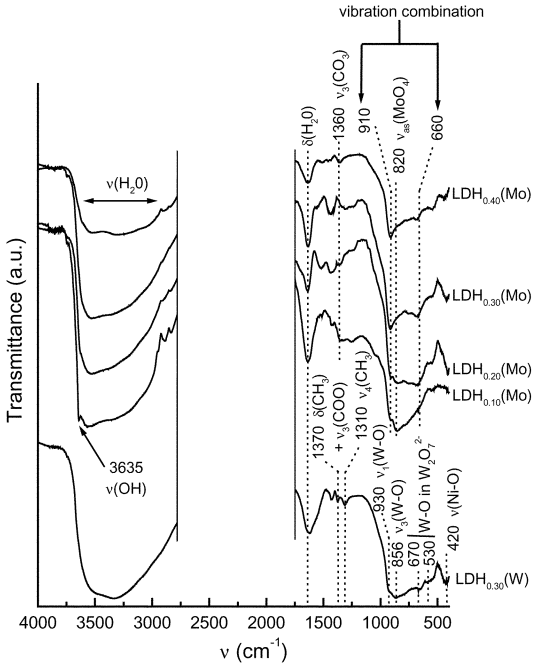

Fig. 2 IR spectroscopy spectra of $LDH_y(Mo)$ (y = 0.10–0.40) and $LDH_{0.30}(W)$. The oscillations between 1750 and 2750 cm^{-1}, which are due to artefacts resulting from the diffuse reflectance technique and do not correspond to the materials, are not shown.

IR spectroscopy of the materials obtained by direct reduction

The IR spectra of the $LDH_y(Mo)$ (y = 0.10–0.40) and $LDH_{0.30}(W)$ phases, are reported in Fig. 2. The general shape of the spectra of the $LDH_y(Mo)$ and $LDH_{0.30}(W)$ phases is similar to that of the $LDH(CO_3)$ phase, which has already been extensively discussed in previous papers.[28,29] The wide band around 3400 cm^{-1} corresponds to the $\nu(H_2O)$ vibration mode of the water molecules, mainly intercalated within the interslab space.

$LDH_y(Mo)$. In this case, Fig. 2 shows that only the spectrum of $LDH_{0.10}(Mo)$ exhibits the narrow $\nu(OH)$ band at 3635 cm^{-1}, which characterises free OH groups.[30] This result is in agreement with XRD, which shows an interstratified structure only for this material. All the $LDH_y(Mo)$ spectra exhibit a very weak band at 1360 cm^{-1}, which is characteristic of carbonate anions in D_{3h} symmetry. Nevertheless, the weak intensity of this band, in comparison with that found in $LDH(CO_3)$, suggests that the carbonate anion amount in the interslab space can be considered as negligible, all the more as a large fraction of these carbonate anions may be adsorbed on the surface of the particles. The band at 820 cm^{-1}, reported in the literature, characterises the existence of molybdenum atoms, which are surrounded by four oxygen atoms in tetrahedral configuration.[31–33] The bands at 910 and 660 cm^{-1} are attributed in the literature to vibration combinations, due to MoO_4 species.[34]

$LDH_y(W)$. As shown in Fig. 2, the absence of any band at 1360 cm^{-1}, which would be characteristic of the presence of carbonate ions (in D_{3h} symmetry), indicates that no parasitic carbonate ion has been inserted, which confirms the results of XRD and chemical analysis, presented in previous sections. The presence of two bands at 1370 and 1310 cm^{-1}, which correspond to the $\delta(CH_3)$ and $\nu_3(COO)$ modes, for the former one, and to the $\nu_4(CH_3)$ mode for the latter one,[35] confirms that

some acetate anions are intercalated in the interslab space or adsorbed at the surface of the particles, as previously shown in the chemical analysis section. Between 1000 and 400 cm^{-1}, four bands (reported in the literature) are observed: (i) two bands, at 930 and 856 cm^{-1}, which correspond to the ν_1(W–O) and ν_3(W–O) vibrations, are characteristic of the presence of WO_4^{2-} tetrahedral species;[36,37] (ii) two bands, at 670 and 530 cm^{-1}, with very weak intensities, might be attributed to W–O vibrations in $W_2O_7^{2-}$ entities.[19]

Such entity would be the result of an association of two WO_4^{2-} tetrahedra, linked by a bridging oxygen, as in the $Cr_2O_7^{2-}$ anion.

These IR results do not allow us to conclude about the exact nature of the intercalated tungstate or molybdate species, but show unambiguously that the entities, intercalated in the *chimie douce* LDHs, are based on the organisation of tetrahedral WO_4 or MoO_4 motives.

A comparative XRD and IR study of the materials prepared by anionic exchange reactions of carbonate ions for (Mo, W) oxometalate ions, starting from $LDH_{0.30}(CO_3)$, is presented hereafter.

XRD and IR study of $LDH_{0.30}$(W) and $LDH_{0.30}$(Mo), prepared by anionic exchange from $LDH_{0.30}(CO_3)$

The exchange reaction of carbonate anions for molybdate or tungstate anions was successful, as shown by the evolution of the XRD patterns and of the IR spectra (Fig. 3). The diffraction line related to the 7.7 Å interreticular distance disappears in favour of one at 9.5 Å, which shows the obtainment of $LDH_{0.30}$(Mo) and $LDH_{0.30}$(W). This exchange is confirmed by the evolution of the IR spectra, which show the disappearance of the $\nu_3(CO_3)$ vibrational band, and the appearance of vibrations characteristic of the molybdate or tungstate species. In the case of tungsten, the faster anionic exchange (1 day instead of 2) can be attributed to the reaction medium pH (pH = 5) and to the trapping of the carbonate ions in the $[W_4O_8(O_2)_6(CO_3)]^{6-}$ species.[24]

These results are in agreement with works performed by El Malki *et al.*,[38] Mendiboure *et al.*,[20] Kooli *et al.*[39,40] and Han *et al.*[41] for other systems, which report success in exchanging carbonate ions for sulfate, nitrate, acetate,[38,20] and vanadate[39–41] in suitable acidic media.

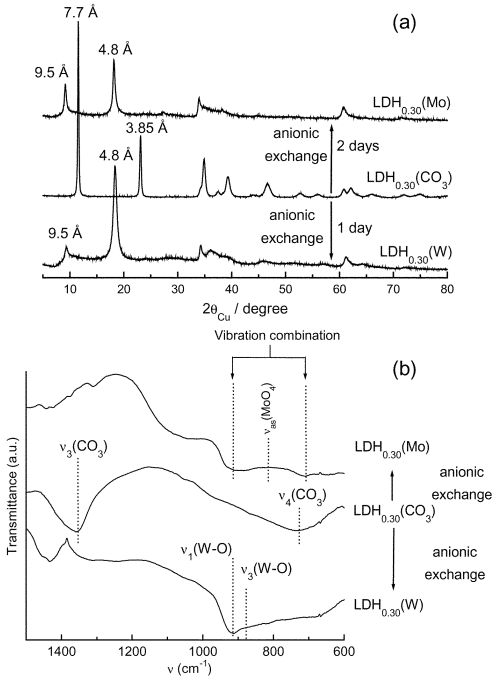

Fig. 3 (a) XRD patterns and (b) IR spectra of $LDH_{0.30}(CO_3)$ and $LDH_{0.30}$(Mo) or $LDH_{0.30}$(W), obtained after the anionic exchange reaction.

X-ray absorption study

EXAFS study. In order to identify the structure of the intercalated species, the study will now focus on $LDH_{0.30}$(Mo) and $LDH_{0.30}$(W), which exhibit no structure interstratification, as shown by XRD and IR spectroscopy. The chemical analysis results suggest that the oxometalate entities are $M_2O_7^{2-}$ (M=Mo, W). The study by X-ray absorption at Ni K-edge, at Mo K-edge for $LDH_{0.30}$(Mo), and at W L(III)-edge for $LDH_{0.30}$(W) is presented hereafter, in order to verify the hypothesis that was made on the intercalated oxometalate entities and to ascertain their precise structural features and arrangement (local environment of molybdenum and tungsten) within the interslab space.

Daresbury software was used to obtain normalised XAFS $\chi(k)$ from X-ray absorption spectra, and the EXCURV suite of programs was used to analyse weighted $k^3\chi(k)$ data. The quality of fit is represented by the R factor which is given by:

$$\sum_i [(1-\sigma_i)(\chi_{i,\mathrm{exp}} - \chi_{i,\mathrm{theor}})] \times 100$$

where i ranges over all the points in the spectrum, σ_i is given by:

$$1/\sigma_i = k_i^3 / \sum_j k_j^3 |\chi_{j,\mathrm{exp}}|$$

and χ_i is the reduced EXAFS function.

All the refinements were performed by systematically considering a first oxygen shell surrounding the metal ions (nickel, molybdenum or tungsten) and by adding gradually the subsequent shells. Except for very special cases, the coordination numbers were always fixed at given values, while the distances, the energy shift and the Debye–Waller factors were refined. The results, obtained for the distances and the Debye–Waller factors, allowed us to validate our chosen models.

Study of the $LDH_{0.30}$(Mo) phase at the Mo K-edge. The Fourier transform of the $k^3\chi(k)$ EXAFS signal obtained at the Mo K-edge is presented in Fig. 4. Two shells, corresponding to

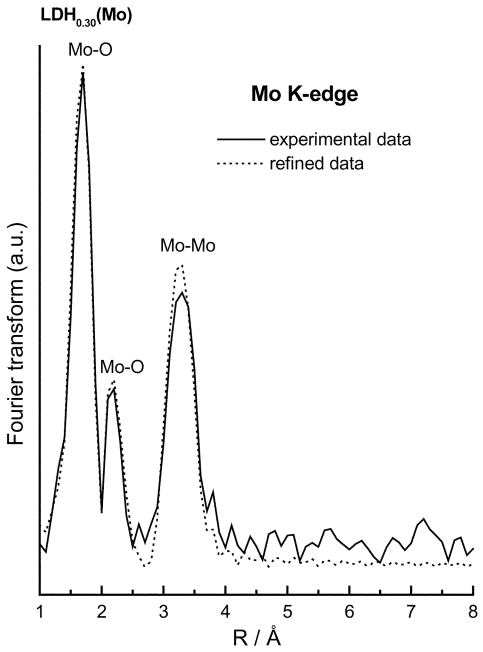

Fig. 4 Fourier transform of the Mo K-edge EXAFS spectrum for the $LDH_{0.30}$(Mo) phase.

oxygen first and second neighbours and one shell corresponding to molybdenum neighbours are clearly shown on the Fourier transform. The various parameter values, obtained after refinement, are gathered in Table S1.†

First calculations of the first shell were performed by fixing the coordination number of molybdenum at 6, and then at 4 (oxygen neighbours). For the 6 coordination number, the refinement is not acceptable, because the Debye–Waller factor is too high ($2\sigma^2 = 0.017$ Å^2) and the fitting index remains too high. When the coordination number is fixed at 4 neighbours, the accordance between the experimental data and the calculated ones is better, and the Debye–Waller factor is lowered ($2\sigma^2 = 0.011$ Å^2). In a second step, on the basis of the 4 neighbours hypothesis, the refinement was carried out by considering a distorted tetrahedron, with three equal short Mo–O bonds and a longer one; the results are thus significantly improved for the R and the Debye–Waller factors ($2\sigma^2 = 0.011$ Å^2 for the regular tetrahedron, $2\sigma^2 = 0.007$ Å^2 and $2\sigma^2 = 0.008$ Å^2 for the distorted tetrahedron). It can therefore be deduced that the first shell is constituted of three oxygen atoms at 1.72 Å and one oxygen atom at 1.93 Å, which corresponds to a distorted tetrahedral oxygen environment for molybdenum. The experimental distances are consistent with the Mo–O distances in the Mo_2O_7 entity found in $MgMo_2O_7$ (1.74 Å and 1.88 Å).[27]

The refinement for the second shell leads to two oxygen neighbours, with a 2.23 Å Mo–O distance ($2\sigma^2 = 0.012$ Å^2). This distance corresponds to an oxygen pointing towards a triangular face of MoO_4 tetrahedra.

The calculation has shown that the third shell is constituted of one molybdenum neighbour. The Mo–Mo distance obtained after simulation (3.25 Å) is consistent with the Mo–Mo distance in $MgMo_2O_7$ (3.31 Å). In this material, the $Mo_2O_7^{2-}$ anion results from the association of two MoO_4 tetrahedra, linked by one oxygen. It can be noticed that the Debye–Waller factor obtained for this molybdenum shell is very small ($2\sigma^2 = 0.005$ Å^2), which indicates the existence of a fixed Mo–Mo distance, and confirms therefore the presence of such $Mo_2O_7^{2-}$ entities in our material.

To sum up, the intercalated molybdate anions in the $LDH_{0.30}$(Mo) phase are identified as $Mo_2O_7^{2-}$ entities, constituted of two MoO_4 distorted tetrahedra, with three short Mo–O bonds (1.72 Å) and a long bridging one (1.93 Å). No Mo–Ni shells were detected.

Study of the $LDH_{0.30}$(Mo) phase at the Ni K-edge. The Fourier transform of the EXAFS oscillations obtained at the Ni K-edge is represented in Fig. 5. The Fourier transform shows 4 main shells. The simulation results are summarised in Table S1.† The first shell is constituted of 6 oxygen neighbours at 2.03 Å ($2\sigma^2 = 0.013$ Å^2) and the next three shells are constituted of 6 nickel neighbours at 3.01 Å ($2\sigma^2 = 0.017$ Å^2), 5.17 Å ($2\sigma^2 = 0.035$ Å^2) and 6.19 Å ($2\sigma^2 = 0.018$ Å^2), respectively. These distances are characteristic of divalent nickel cations, located in edge-sharing octahedra of the slab; they are in good agreement with those calculated from the a_{hex} parameter ($d_{Ni-Ni} = 3.04$ Å, 5.26 Å and 6.08 Å) and with previous studies.[42–45]

Besides, the refinement did not evidence the existence of molybdenum neighbours for nickel. This behaviour is in agreement with the fact that no nickel atom was detected as molybdenum neighbour at the Mo K-edge. This suggests that the molybdenum atoms are not precisely located in one defined site in the interslab space. This behaviour will be commented on in the Discussion section. The detection of a Ni shell around nickel at rather long distance (6.19 Å) is due to multiple scattering at the Ni-edge, due to the presence of linear Ni–Ni–Ni chains. It implies a significant increase of the Fourier transform amplitude for the Ni–Ni distance, which is around twice the value of the a_{hex} cell parameter.

Study of the $LDH_{0.30}$(W) phase at the W L(III)-edge. The Fourier transform of the EXAFS oscillations at the W L(III)-edge is shown in Fig. 6. The EXAFS data are poorer for $LDH_{0.30}$(W) than for $LDH_{0.30}$(Mo), so that the accordance between the experimental and calculated data is not as good as in the case of the $LDH_{0.30}$(Mo) phase. The refinement based on 6 oxygen neighbours for the first shell is not relevant, while the result is acceptable with a tetrahedral environment (R decreases significantly, and $2\sigma^2$ decreases from 0.020 Å^2 to 0.011 Å^2). As in the case of $LDH_{0.30}$(Mo), the refinement of the EXAFS data shows that the first shell around tungsten atoms is composed of three oxygen atoms located at a distance of 1.74 Å, and one oxygen atom at a distance of 1.95 Å (Table S2†). The R and the Debye–Waller factors are quite good ($2\sigma^2 = 0.007$ Å^2 and

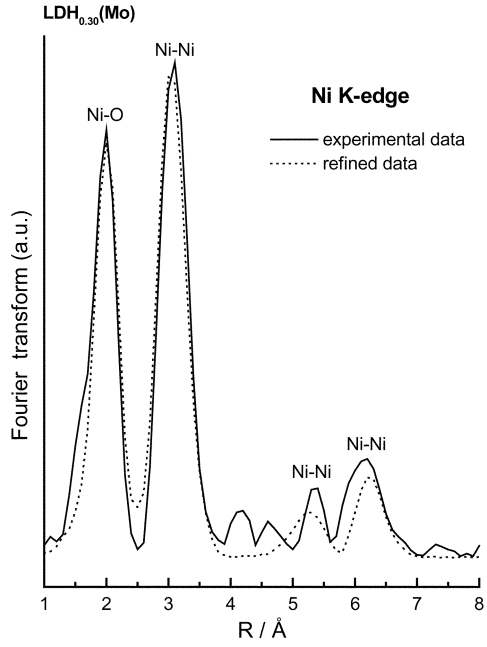

Fig. 5 Fourier transform of the Ni K-edge EXAFS spectrum for the $LDH_{0.30}$(Mo) phase.

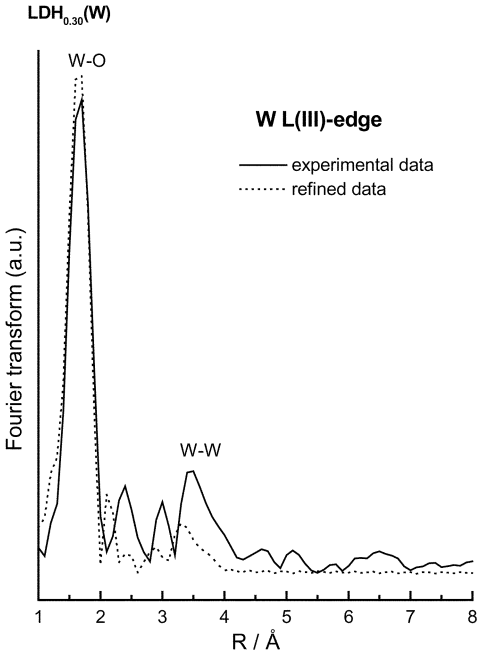

Fig. 6 Fourier transform of the W L(III)-edge EXAFS spectrum for the $LDH_{0.30}$(W) phase.

$2\sigma^2 = 0.006$ Å^2, respectively). These results suggest that tungsten is in a distorted tetrahedral environment, as in the case of $LDH_{0.30}$(Mo). These distances are close to those reported for tungsten, located in tetrahedral environment, in the $Ag_2W_2O_7$ compound (1.72 Å and 1.92 Å).[46] Besides, the refinement shows that each tungsten has one tungsten neighbour with a short W–W distance, equal to 3.20 Å. These overall results suggest that $LDH_{0.30}$(W) contains intercalated $W_2O_7^{2-}$ species, based on the same structural model as $Mo_2O_7^{2-}$, *i.e.* two WO_4 distorted tetrahedra, linked by one oxygen atom. It should be noted that the Debye–Waller factor is quite high ($2\sigma^2 = 0.019$ Å^2) for the W–W shell, leading to the conclusion of an occurrence of a large disorder within the interslab space. Besides, the adequacy between the deduced and calculated Fourier transform (Fig. 6) can be improved by introducing a large number of oxygen atoms (10–12), located at rather long distances far from tungsten ($\approx$3.50 Å). This allows to take the peak in the Fourier transform in the range 3–4 Å, into better account. These oxygen atoms might belong to the slab, to the interlamellar water or to the acetate anions, which were inserted during the material synthesis. Nevertheless, probably due to the disorder of the species within the interslab space, the experimental data are not good enough to lead to a significant and precise refinement of the tungsten coordination number and of the W–O distances.

In conclusion, as in the case of $LDH_{0.30}$(Mo), the EXAFS data show that the inserted tungstate anions in the $LDH_{0.30}$(W) phase are $W_2O_7^{2-}$ entities, based on the association of two WO_4 distorted tetrahedra, with a long W–O bond (1.95 Å) and three short ones (1.74 Å).

Discussion about the structure

The overall results, coming from various characterisation techniques, have shown that the $LDH_{0.30}$(W) and $LDH_{0.30}$(Mo) phases contain $M_2O_7^{2-}$ entities (M=Mo, W), inserted in the interslab space. In particular, the study of the local environment of the oxometalate species by X-ray absorption spectroscopy has revealed the presence of tetrahedral entities in the two cases. The relatively short metal–metal distance shows that these tetrahedra must share one of their oxygens, in agreement with the IR and chemical analysis data, which also suggest the existence of $M_2O_7^{2-}$ entities. From the M–M distance, the relative positions of the tetrahedra in the $M_2O_7^{2-}$ entities can be determined. The M–O–M angle, close to 115° in both cases, leads to propose a shape, drawn in Fig. 7, which shows that the $M_2O_7^{2-}$ entities can be considered as cylinders.

These cylinders can rotate around their revolution axis, so that the $M_2O_7^{2-}$ entities can exhibit several orientations within the interslab space. Nevertheless, in a first approximation, the thickness of these entities always corresponds to two oxygen layers. The orientation of the inserted species is therefore in full accordance with the interslab distances given by XRD, 9.4 Å for $LDH_{0.30}$(W) and 9.6 Å for $LDH_{0.30}$(Mo), which are compatible with the presence of two oxygen-atom layers in the interslab space. Similar results were proposed by Malherbe *et al.* in their study of $Cr_2O_7^{2-}$ intercalated LDHs.[47]

In the EXAFS study of $LDH_{0.30}$(Mo), a second shell of two oxygen atoms, surrounding molybdenum at 2.23 Å, was found. As previously mentioned, one can assume that these oxygen atoms point towards a triangular face of MoO_4 tetrahedra. This oxygen atom can belong either to a (Ni, Co)O_2 slab, or to a water molecule. The first hypothesis is not likely to occur since it would lead to a fixed orientation of the MoO_4 tetrahedra with regard to the (Ni, Co)O_6 octahedra, and therefore, to a quite ordered structure. The second hypothesis, involving water molecules, seems quite reasonable since the water molecules are not in a fixed position in the interslab space. Moreover, the chemical analysis leads to 0.74 H_2O molecules and 0.15 $Mo_2O_7^{2-}$ entities in the interslab space, which is in good agreement with two oxygen neighbours around molybdenum, as found in the second shell refinement.

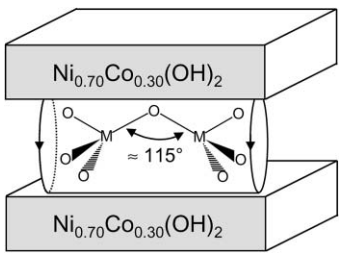

Fig. 7 Scheme of $M_2O_7^{2-}$ entities in the LDHs.

As shown in Fig. 1, the intensities of the first two diffraction lines of LDHs, intercalated with oxometalate (Mo, W) species, are inverted, when compared to $LDH_{0.30}(CO_3)$. In order to understand this behaviour, a simulation of the XRD patterns of the LDH phases was performed, with the DIFFaX program,[48] as a function of tungsten or molybdenum amounts within the interslab space. For the simulation, a centrosymmetric NiO_2 slab was built up by using the $-3m$ point symmetry and the following positions for nickel (0, 0, 0) and oxygen atoms (1/3, 2/3, 0.1064). The NiO_2 slabs were then stacked along the c direction on the basis of an AB BC CA packing of the oxygen layers. The hydrogen atoms were neglected, because they are too light to influence the XRD pattern. The overall molybdate (tungstate, respectively) entities were considered as generating a MoO_2 slab (or WO_2 slab), which was built on the same model as NiO_2, with the positions of molybdenum (tungsten, respectively) (0, 0, 0) and oxygen (1/3, 2/3, 0.1585). The molybdenum (tungsten, respectively) plane is thus situated in the centre of the interslab space between two oxygen planes that are at 1.49 Å from the centre. This distance was calculated from the 1.74 Å M–O distance (M=Mo, W), deduced from the X-ray absorption results. This MO_2 slab was considered to be located at the centre of the interslab space. A gaussian function was used for the profile simulation. Fig. 8 presents a scheme of such a configuration as well as the evolution of the diffraction lines (in the 5–30° range), for Mo : Ni (W : Ni respectively) molar ratios ranging from 0 to 1. The XRD patterns were simulated in the ratio from 0 to 1 in order to have an overall view of the change in the line intensity, even if the largest values do not correspond to real materials. As shown in Fig. 8, the intensities of the first two lines tend to reverse themselves with increasing molybdenum amount. The line intensities are inverted for a 0.45 Mo : Ni molar ratio. A good agreement is obtained between the experimental XRD pattern and the diagram that was calculated for a 0.5 Mo : Ni molar ratio. This value is significantly different from the experimental value, 0.30, deduced from chemical analysis. It should be noted that, in this simulation, the description of the structure of the interslab space is very far from the real one, which is unknown. The shape, the orientation and the exact position of the $Mo_2O_7^{2-}$ entity and the presence of water molecules are not considered. Besides, the overall composition of the interslab space was described as $(MoO_2)_n$, instead of $(Mo_2O_7)_{0.15}(H_2O)_{0.74}$. Nevertheless, this crude simulation explains why the intensities of the (001) and (002) diffraction lines are inverted.

In the case of the LDH_y(W) phases (Fig. 8), the simulation shows a decrease, followed by an increase of the first peak intensity, while the second peak intensity continuously increases when an increasing tungsten amount is introduced in the interslab space. An inversion of the intensities of the first two peaks is observed for a W : Ni molar ratio higher than 0.25. A good agreement is obtained between the experimental XRD and the diagram that was calculated for a 0.3 W : Ni molar ratio. This value is closed to the experimental value, 0.26, deduced from the chemical analysis.

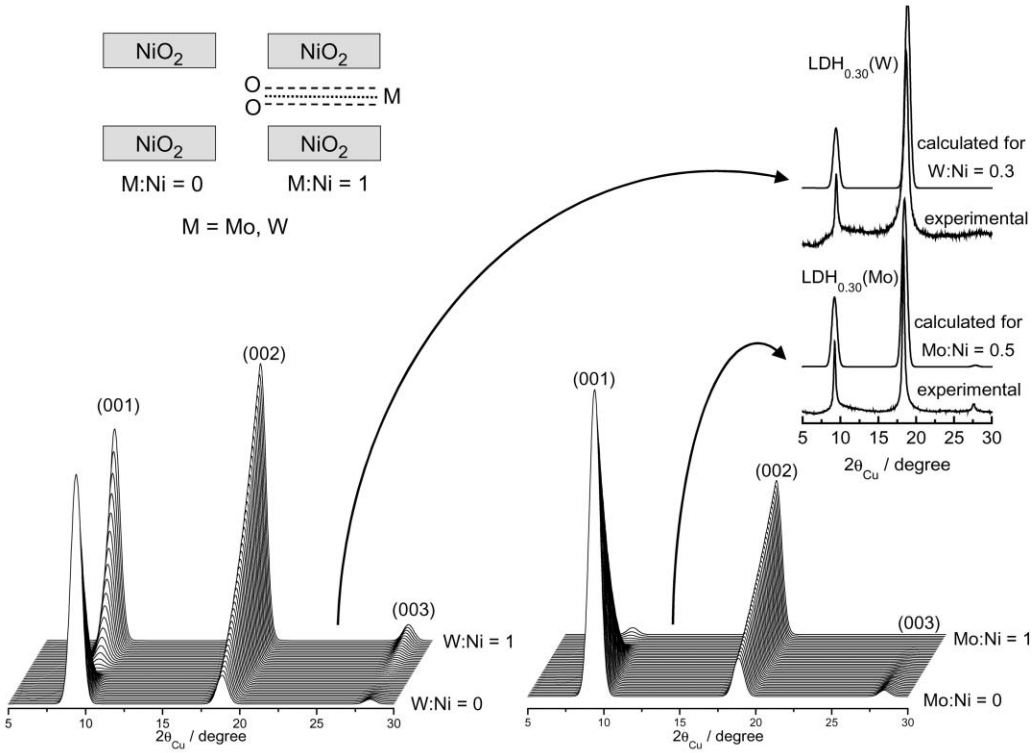

Fig. 8 Simulated XRD patterns of LDH_y(Mo) and LDH_y(W) *versus* M : Ni ratio (M=Mo, W) in the material. A hypothetical structure with NiO_2, xMO_2 formula has been assumed. The MO_2 slab inserted between the NiO_2 slabs, consists of three successive (O, M, O)layers.

It should be noted that, in the XRD patterns of the $LDH_{0.30}$-(Mo) phase, the (003) line appears with a very low intensity, while it does not appear in the case of the homologous tungstate phase. At first sight, this difference could appear as surprising, but in fact, it is in accordance with the simulations, reported in Fig. 8.

The last point, which must be discussed, concerns the existence of a turbostratic-like behaviour of $Mo_2O_7^{2-}$ and $W_2O_7^{2-}$ intercalated phases, while in the case of carbonate intercalated phases (Fig. 1) a unit cell can be deduced. In this latter case, the CO_3^{2-} anions occupy well defined sites,[49] this entails a long range ordering in the interslab space. However, on the contrary, the large size of the $M_2O_7^{2-}$ entities, their peculiar shape (which leads to misorientation), the presence of water molecules (pointing towards the face of the tetrahedra), and their hydrogen bonding leads to a disordered distribution of intercalated species, which prevents the existence of an ideal packing of the slabs and therefore induces local distortions, which lead to the turbostratic shape of the XRD patterns.

Conclusion

The present study has shown that new layered double hydroxides, intercalated with oxometalate (Mo, W) species, were obtained by *chimie douce* reactions. All the characterisation techniques have revealed that these entities are $M_2O_7^{2-}$ anions (M=Mo, W) based on MO_4 tetrahedra linked by a bridging oxygen. Simulations of the XRD patterns of LDHs have allowed the inversion in intensity of the first two (00*l*) diffraction lines, which is rather unusual for LDHs, to be addressed. It is due to the location of a significant amount of molybdenum or tungsten, which are heavy species, at the centre of the interslab space.

Further experiments have shown that these materials exhibit a very interesting thermal behaviour, which will be the subject of a future publication.

Acknowledgement

We wish to thank M. Basterreix for her technical support. We gratefully acknowledge the help of the staff of LURE.

References

1 F. Canavi, F. Trifiro and A. Vaccari, *Catal. Today*, 1991, **11**, 173.
2 A. Vaccari, *Catal. Today*, 1998, **41**, 53.
3 V. Rives and M. A. Ulibarri, *Coord. Chem. Rev.*, 1999, **181**, 61.
4 C. Delmas and Y. Borthomieu, *J. Solid State Chem.*, 1993, **104**, 345.
5 K. S. Han, L. Guerlou-Demourgues and C. Delmas, *Solid State Ionics*, 1996, **84**, 227.
6 C. Vaysse, L. Guerlou-Demourgues, C. Delmas and E. Duguet, *Macromolecules*, 2001, in preparation.
7 J. J. Braconnier, C. Delmas, C. Fouassier, M. Figlarz, B. Beaudoin and P. Hagenmuller, *Rev. Chim. Miner.*, 1984, **21**, 496.
8 C. Delmas, J. J. Braconnier, Y. Borthomieu and P. Hagenmuller, *Mater. Res. Bull.*, 1987, **22**, 741.
9 L. Demourgues-Guerlou, J. J. Braconnier and C. Delmas, *J. Solid State Chem.*, 1993, **104**, 359.
10 B. Sels, D. De Vos, P. J. Grobet, F. Pierard, A. Kirsch-De Mesmaeker and P. Jacobs, *J. Phys. Chem. B*, 1999, **103**, 11114.
11 B. Sels, D. De Vos, M. Buntinx, F. Pierard, A. Kirsch-De Mesmaeker and P. Jacobs, *Nature*, 1999, **400**, 855.
12 E. Gardner and T. J. Pinnavaia, *Appl. Catal., A*, 1998, **167**, 65.
13 T. Tatsumi, K. Yamamoto, H. Tajima and H. Tominaga, *Chem. Lett.*, 1992, 815.
14 M. A. Drezdzon, *Inorg. Chem.*, 1988, **27**, 4628.
15 J. Twu and P. K. Dutta, *Chem. Mater.*, 1992, **4**, 398.
16 H. Nijs, M. De Bock and E. F. Vansant, *J. Porous Mater.*, 1999, **6**, 101.
17 C. Delmas, J. J. Braconnier, Y. Borthomieu and M. Figlarz, *Solid State Ionics*, 1988, **28–30**, 1132.
18 S. Veil, *C. R. Acad. Sci. Paris*, 1925, 932.
19 N. J. Campbell, A. C. Dengel, C. J. Edwards and W. P. Griffith, *J. Chem. Soc., Dalton Trans.*, 1989, 1203.
20 A. Mendiboure and R. Schöllhorn, *Rev. Chim. Miner.*, 1986, **23**, 819.
21 C. Delmas, C. Fouassier and P. Hagenmuller, *Physica B*, 1980, **99**, 81.
22 C. Delmas, Y. Borthomieu, C. Faure, A. Delahaye and M. Figlarz, *Solid State Ionics*, 1989, **32/33**, 104.

23 S. Rey, J. Merida-Robles, K. S. Han, L. Guerlou-Demourgues, C. Delmas and E. Duguet, *Polym. Int.*, 1999, **48**, 277.
24 R. Stomberg, *Acta Chem. Scand. Ser. A*, 1985, **39**, 507.
25 L. Guerlou-Demourgues, C. Denage and C. Delmas, *J. Power Sources*, 1994, **52**, 269.
26 L. Guerlou-Demourgues and C. Delmas, *J. Power Sources*, 1994, **52**, 275.
27 K. Stadnicka, J. Haber and R. Kozlowski, *Acta Crystallogr., Sect. B*, 1977, **33**, 3859.
28 C. Faure, Y. Borthomieu, C. Delmas and C. Fouassier, *J. Power Sources*, 1991, **36**, 113.
29 C. Faure, C. Delmas, C. Fouassier and P. Willmann, *J. Power Sources*, 1991, **35**, 249.
30 C. Faure, C. Delmas and P. Willmann, *J. Power Sources*, 1991, **35**, 263.
31 J. Hanuza, A. Benzar, A. Haznar, M. Maczka, A. Pietraszko, J. H. Van der Maas and E. T. G. Lutz, *Vib. Spectrosc.*, 1996, **12**, 25.
32 J. Hanuza, M. Maczka, K. Hermanowicz, P. J. Deren, W. Streck, L. Folcik and H. Drulis, *J. Solid State Chem.*, 1999, **148**, 468.
33 M. Maczka, J. Hanuza, E. T. G. Lutz and J. H. Van der Maas, *J. Solid State Chem.*, 1999, **145**, 751.
34 J. Hanuza, A. Haznar, M. Mackza, A. Pietraszko, A. Lemiec, J. H. Van der Maas and E. T. G. Lutz, *J. Raman Spectrosc.*, 1997, **28**, 953.
35 K. Nakamoto, in *Infrared and Raman spectra of inorganics and coordination compounds*, Wiley-Interscience, New York, 1997.
36 R. H. Busey and O. L. J. Keller, *J. Chem. Phys.*, 1964, **41**, 215.
37 L. J. Burcham and I. E. Wachs, *Spectrochim. Acta, Part A*, 1998, **54**, 1355.
38 K. E. Malki, A. De Roy and J. P. Besse, *Eur. J. Solid State Inorg. Chem.*, 1989, **26**, 339.
39 F. Kooli, V. Rives and M. A. Ulibarri, *Inorg. Chem.*, 1995, **34**, 5114.
40 F. Kooli, V. Rives and M. A. Ulibarri, *Inorg. Chem.*, 1995, **34**, 5122.
41 K. S. Han, L. Guerlou-Demourgues and C. Delmas, *Solid State Ionics*, 1997, **98**, 85.
42 K. I. Pandya, W. E. O'Grady, D. A. Corrigan, J. McBreen and R. W. Hoffman, *J. Phys. Chem.*, 1990, **94**, 21.
43 B. C. Cornilsen, X. Shan and P. L. Loyselle, *Proc. Electrochem. Soc.*, 1990, **90–4**, 82.
44 A. N. Mansour and C. A. Melendres, *J. Phys. Chem. A*, 1998, **102**, 65.
45 C. Tessier, L. Guerlou-Demourgues, C. Faure, A. Demourgues and C. Delmas, *J. Mater. Chem.*, 2000, **10**, 1185.
46 B. M. Gatehouse and P. Leverett, *J. Chem. Soc., Dalton Trans.*, 1976, 1316.
47 F. Malherbe, L. Bigey, C. Forano, A. De Roy and J. P. Besse, *J. Chem. Soc., Dalton Trans.*, 1999, 3831.
48 M. Treacy, J. Newsam and M. Deem, *Proc. R. Soc. London, Ser. A*, 1991, **43**, 499.
49 S. A. Solin, D. R. Hines, G. T. Seidler and M. M. J. Treacy, *J. Phys. Chem. Solids*, 1996, **57**, 1043.